27 Feb 2023

Calculations of Adsorption-Dependent Refractive Indices of Metal-Organic Frameworks for Gas Sensing Applications

Nahideh Salehifar

Peter Holtmann

Abhishek Prakash Hungund

Homayoon Soleimani Dinani

et. al. For a complete list of authors, see https://scholarsmine.mst.edu/ele_comeng_facwork/4737

Recommended Citation

N. Salehifar et al., "Calculations of Adsorption-Dependent Refractive Indices of Metal-Organic Frameworks for Gas Sensing Applications," *Optics Express*, vol. 31, no. 5, pp. 7947 - 7965, Optica, Feb 2023.
The definitive version is available at https://doi.org/10.1364/OE.478427

Research Article Vol. 31, No. 5 / 27 Feb 2023 / Optics Express 7947
Optics EXPRESS

Calculations of adsorption-dependent refractive indices of metal-organic frameworks for gas sensing applications

NAHIDEH SALEHIFAR, PETER HOLTMANN, ABHISHEK PRAKASH HUNGUND, HOMAYOON SOLEIMANI DINANI, REX E. GERALD II, AND JIE HUANG*

Department of Electrical and Computer Engineering, Missouri University of Science and Technology, 141 Emerson Electric Co. Hall, 301 W. 16th., Rolla, Missouri 65409, USA
jieh@mst.edu

Abstract: Detection of volatile organic compounds (VOCs) is one of the most challenging tasks in modelling breath analyzers because of their low concentrations (parts-per-billion (ppb) to parts-per-million (ppm)) in breath and the high humidity levels in exhaled breaths. The refractive index is one of the crucial optical properties of metal-organic frameworks (MOFs), which is changeable via the variation of gas species and concentrations that can be utilized as gas detectors. Herein, for the first time, we used Lorentz–Lorentz, Maxwell–Ga, and Bruggeman effective medium approximation (EMA) equations to compute the percentage change in the index of refraction (Δn%) of ZIF-7, ZIF-8, ZIF-90, MIL-101(Cr) and HKUST-1 upon exposure to ethanol at various partial pressures. We also determined the enhancement factors of the mentioned MOFs to assess the storage capability of MOFs and the biosensors' selectivity through guest-host interactions, especially, at low guest concentrations.

1. Introduction

Advances in the design and synthesis of metal-organic frameworks (MOFs), film preparation processes, and examinations of their physicochemical characteristics have supported progress in developing MOF-based gas sensors during the last two decades [1–3]. MOFs are excellent gas-sensing materials with applications in monitoring volatile organic compounds (VOCs) in human breath, medical diagnostics, gas storage and separation, industrial gas leaks, and other fan individual's health [4–8]. Phillips [9] used gas chromatography-mass spectrometry (GC-MS) to estimate 1259 VOCs from 20 normal healthy subjects in 1997. Phillips described 3481 VOCs in the breath gas of healthy controls using GC/MS in 1999, with an average of about 200 VOCs detectable in an individual's breath gas. Exhaled breath gas compounds are generally classified into 3 groups including inorganic compounds such as nitric oxide, and condensates, which contain hydrogen peroxide, and VOCs. A significant proportion of breath VOCs has nanomolar (10^{-9}) and picomolar (10^{-12}) concentration ranges, requiring the use of highly sensitive instruments. The major VOCs in the breath of healthy individuals are 2-methyl pentane (10.8 ppb to 80 ppt), hexane (12.86 ppb to 290 ppt), 1-butanol (750 ppt), octane (1.29 ppb to 100 ppt), isoprene (580 ppb to 12 ppb), acetone (1880 ppb to 1.2 ppb), ethanol (1000 ppb to 13 ppb), methanol (2000 ppb to 160 ppb), and other alcohols [10,11].

The main important challenges for VOC measurements are their low concentrations in exhaled breath and the high humidity level present in human breath that undoubtedly adversely affect the measurement results of some analytical techniques such as GC-MS and others [12,13]. Several techniques have been developed to monitor and analyze the VOCs in human exhaled breath. The following technologies are used in breath tests: Gas Chromatography and GC–MS, Proton-Transfer Reaction-Mass Spectrometry (PTR-MS), Selected Ion Flow Tube-Mass Spectrometry

#478427 https://doi.org/10.1364/OE.478427
Journal © 2023 Received 26 Oct 2022; revised 20 Dec 2022; accepted 27 Dec 2022; published 17 Feb 2023

Optics EXPRESS

(SIFT-MS), Sensor Arrays and Electronic Noses (eNoses), Ion-Mobility Spectrometry (IMS), and Optical Absorption [10]. GC-MS has a high reliability, sensitivity, and durability level, and it can provide additional data on biological samples that consist of specific VOCs [14]. PTR-MS [15] is more sensitive than GC-MS in identifying VOC concentrations down to ppt and ppb levels, and it does not require the time-consuming pre-concentration phase. Like PTR-MS, SIFT-MS [16] affords fast performance in analyzing exhaled breath measurements. SIFT-MS applies a chemical ionization method using positive precursor ion source generation. In SIFT-MS, the ion-molecule reactions produce distinctive product ions that match up to each detectable gas species in the sample. These product ions are mass-sorted and counted by a downstream detection system. SIFT-MS has been used for polar substances and unsaturated hydrocarbons such as isoprene and acetone.

Furthermore, one of the most important sensor-based techniques in clinical practice is the e-Nose, which includes several non-selective gas sensors and pattern algorithms [17]. IMS is another quick technique for detecting volatile compounds at very low concentrations (ppm-ppb) without the need for pre-concentration. It is based on calculating how long it takes an ion to travel through a drift tube [18]. Once a group of specific molecules is associated with a disease, then optical instruments can be used to identify the disease. These instruments are highly selective and can be employed to conduct the online real-time ppb-level evaluation of selected molecules [10].

Additionally, in practical applications, the long-term sensing stability of MOF-based VOCs detectors may be another challenge [19,20]. MOF-based sensors have low sensing ability and high operating costs at standard temperature and pressure (STP) due to high desorption temperatures and significant pressure drops [21]. When the external environmental conditions change, such as increasing the temperature or decreasing the pressure, the VOC molecules within the adsorbents are more likely to be released or exhibit a relatively insignificant amount of adsorption. Consequently, the sensing performance of the sensors will be harmed [22–24]. More work is needed to address the issues that are preventing MOF-based sensors from becoming mass-produced and commercialized, which can, in turn, limit their applications as biomarker sensors [25,26]. A wide range of VOC biomarker sensors can be categorized by signal transduction, including electrical, optical, and acoustic [27–29]. Solvatochromism is one of the most powerful means of transducing a sensed signal by measuring the visible change in a material's color caused by a large shift in the sample's absorption spectrum [29]. Luminescence sensing with MOFs is another method that is accomplished by enhancing, quenching, or altering fluorescence signals as a response to the target adsorption. Although luminous MOF sensors have been effectively used to detect oxygen-based explosive substances in a variety of aromatic compounds and amines, there are just a few published examples of biological sensing applications [29–33].

Interferometry [34,35], Localized Surface Plasmon Resonance (LSRP) [36], and Colloidal Crystals [35] differ from luminescence and solvatochromic measurements in that they do not include light absorption or emission by the MOF. These devices are reported as accurate, simple, adaptable, and noise-resistant ways to identify gas molecules. The methods mentioned above are based on the refractive index (RI) change of the MOF as a result of the interactions between the guest molecules (gas molecules) and the host (MOF) that result in guest adsorption. The refractive index is a measure of the interaction of light with polarizable matter, and it rises with the number of polarizable electrons and their polarizability. Changes in the RI of the MOF can be caused by the composite, volume (Vol)-weighted property of empty framework (RI = 1 for empty pores), and adsorbed guest. Variations in the RI can make a shift in the visible extinction spectrum in LSPR spectroscopy. As the pores gradually fill and the space inside the MOFs ($n = 1$) is replaced by adsorbate molecules (VOCs), the refractive index (n) of the MOF increases ($n > 1$). This process enables the identification of small VOC molecules with extremely small differences in RIs [37–43]. However, only a few reports have been published in this area, and

Optics EXPRESS

they show mostly RI changes due to adsorbing hydrocarbons, alcohols, and water. The lack of enough research in RI gas sensors strongly raises the need to find suitable methods for calculating and simulating RI changes upon adsorbing small concentrations of various VOCs inside MOFs.

Using a combination of optical fibers and sensitive hydrophobic thin films to develop different chemical sensing platforms is one possible solution for creating a water suppression sensor to detect human exhalaled gases. For humidified gas-sensing applications, high-performance hydrophobic MOFs, especially the zeolitic imidazolate framework (ZIF) category (e.g., ZIF-8) can be coated on the cleaved end facet of an optical fiber using a variety of chemical and physical methods to make sensors that repel water. The adsorption and desorption isotherms for hydrophobic MOFs exhibit a hysteresis loop, demonstrating that MOF cage windows act to produce a water adsorption restriction [4]. The analysis of water molecules as spectator interferents in ZIF-8 demonstrated that ZIF-8 functioned well as a very hydrophobic MOF [33]. Thus, water adsorption by ZIF-8 or other hydrophobic MOFs under ambient conditions is not problematic [4]. For example, the analysis of ethanol guest molecules in ZIF-8 is interesting because several studies illustrate the effect of large guest molecule adsorption capacities and the associated problems of spectator interferents [33–36].

As discussed above another main issue facing the production of biosensors for the direct detection of diseases is their low sensitivity in real-time, an issue that still needs improvement [38]. For example, as mentioned above many researchers have conducted studies measuring ethanol concentrations in human exhaled breaths over long periods using various methods such as SIFT-MS. According to the results, there are significant differences between the concentrations of ethanol in the breaths of healthy individuals and those who are suffering from select diseases, as listed in Table 1. However, as we can see, the range of ethanol in all listed diseases is in the ppb range, making any means of measuring the concentrations quite difficult.

Table 1. The relevant ranges of ethanol in VOC panels that indicate various diseases [44–47]

Disease	Range (Ave)
Healthy Person	209 ppb
Diabetes	9.6–45.0 ppb
Lung Cancer	466.9 ppb
DCIS (Breast Cancer)	917 ppb
Larynx Cancer	540 ppb
Benign Tumor	458 ppb
Luminal A (Breast Cancer)	336 ppb
Luminal B (Breast Cancer)	400 ppb
Triple Negative (Breast Cancer)	397 ppb
HER2-Positive Breast Cancer	480 ppb

Due to having a high surface area, MOFs can concentrate various types of VOCs into the pores, enhancing the detector sensitivity. MOFs' uniform and tunable pore sizes also contribute to biosensors' selectivity through guest-host interactions. Selectivity is one of the most significant characteristics of a biosensor, particularly regarding human breath analyzers, where the diagnoses of various diseases may depend on measuring abnormally high levels of specific VOCs that are linked to the corresponding diseases.

A key aspect of this paper is the development of the theoretical constructs necessary to predict changes in RI of MOF sensors versus guest loadings. In this research, we developed the fundamental relationship between adsorption isotherms for MOF-based microporous materials and the associated changes in the refractive index. Calculating the variation of the refractive

Optics EXPRESS

index as a function of guest loading can give us a fair idea about the lowest level of detectable VOCs, as well as what instruments or procedures will work best to achieve a very low limit of detection. This research also paves the way for breath analyzer sensors or successful optical fiber-MOF (OF-MOF) sensors for sensing explosives, both of which require sufficient sensitivity for detecting VOCs or explosive molecules under ambient conditions at ppm-level or lower concentrations. Once the sensitivity metric is met, the second requirement is high selectivity for the target VOC or explosive molecule over interferent molecules that may generate incorrect results.

2. Results and discussion

In this section, we will look for changes in the index of refraction caused by ethanol adsorption in various MOFs. To estimate the change, we developed a single formula. However, as shown in the derived formula, we must calculate the occupied volume of all guest types (variable V in Eq. (7)) within the MOFs. For the reasons stated above, we must first determine the average number of ethanol molecules, as an example guest, that can be adsorbed at various partial pressures or concentrations. We can calculate the volume of the adsorbed ethanol molecules once we know how many are adsorbed in the pores. The ethanol adsorption capacities for various MOFs are calculated in the first section (2.1, which is divided into 2 parts), and their change in the index of refraction is estimated in section 2.2, based on the calculated results in parts 2.1.1 and 2.1.2.

2.1. Ethanol adsorption capacities in MOFs

We need to compute some special parameters to characterize MOFs' adsorption capacity and selectivity. The adsorption capacity is defined as the amount of adsorbate taken up by the adsorbent per unit mass (or volume) of the adsorbent. A flow chart for calculating the enhancement factor for a MOF is depicted in Fig. 1. At low pressure (~0.0001 atmosphere), the MOFs cause barely detectable changes in the adsorption isotherm due to the low concentration of guest molecules. In contrast, the MOFs can adsorb a significantly greater number of guest molecules up to saturation, resulting in an obvious RI change of a gas sensor that can be easily detected with high sensitivity.

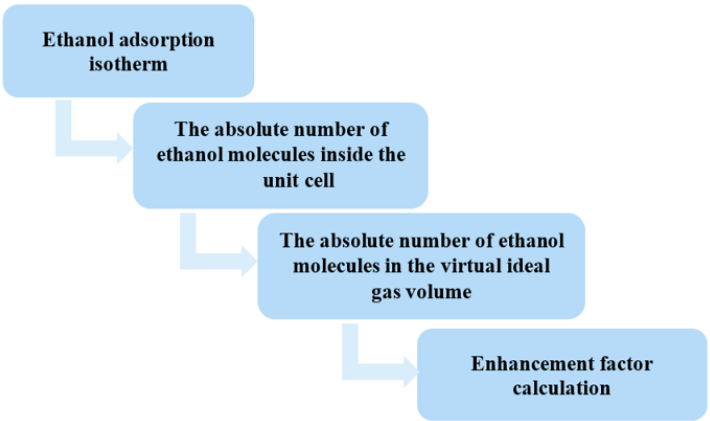

Fig. 1. Flow chart used for enhancement factor calculations.

In the first step of our work, the experimental adsorption isotherms of ethanol at 293 K for ZIF-7, HKUST-1 (Hong Kong University of Science and Technology), MIL-101(Cr) (the chromium terephthalate metal–organic framework), ZIF-90, and ZIF-8 were extracted from the literature to evaluate ethanol adsorption uptakes for varying partial pressures of guests. The unit

Optics EXPRESS

cell volume of each MOF, which is discussed in the following section, is used to calculate the number of gas molecules that can be adsorbed at various concentrations. The guest uptake for the same volume of empty space (without a MOF) can be compared to the adsorption capacities of different MOFs. The adsorption capacities can be influenced by some properties of MOFs such as the pore size, unit cell volume, periodic structure, surface area, host-guest interaction, and more [4,44–46].

2.1.1. Ethanol adsorption capacities in ZIF-8 at room temperature

Schematic drawings of the unit cell volume elements that make up the ZIF-8 MOF single crystal are shown in Fig. 2. An equivalent unit cell virtual (Virt) space volume and a MOF ZIF-8-unit cell volume are compared side-by-side in Fig. 2. The volumes are cubic, with each dimension equal to 1.6992 nm in size. Guest analyte molecules can access the ZIF-8 11.6 Å-diameter pore through 3.4 Å-diameter windows on all six sides of the unit cell. The solid blue pyramids are molecular structural units that define the MOF ZIF-8-unit cell. The solid yellow sphere represents a pore in the unit cell with a diameter of 11.6 Å that can be accessed by guest molecules that pass through 3.4 Å-diameter windows located on all six sides of the unit cell. The virtual cubic volume has an accessible volume of 100% whereas the ZIF-8-unit cell only has an accessible volume of 51% (the pore volume) due to the inaccessible space occupied by the ZIF-8 structure. For the case of ethanol guest molecules (a common test guest molecule), a maximum of approximately 23 molecules can fill (saturate) the ZIF-8 pore. Each unit cell of ZIF-8 consists of 276 atoms with a pore volume of ≈2500 $Å^3$ (Fig. 2). ZIF-8 has been well investigated in terms of the adsorption of various VOCs in bulk powder cases.

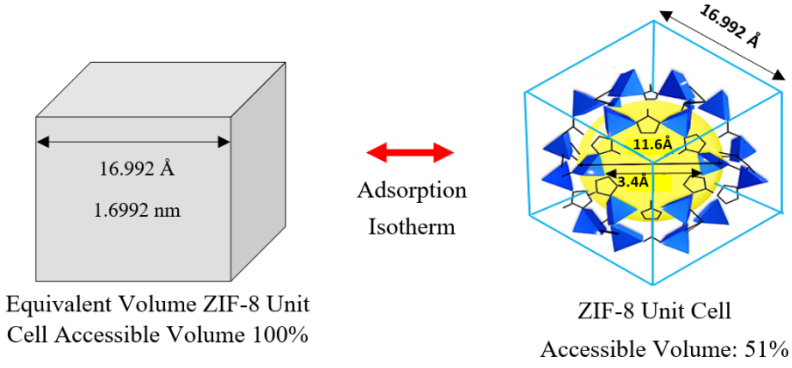

Fig. 2. A schematic drawing of the unit cell volume elements that make up a ZIF-8 single crystal.

Employing the published data points for the room-temperature adsorption isotherm of the ethanol/ZIF-8 guest/host system, we produced Fig. 3 to pictorially illustrate the equilibrium partition of both nitrogen and ethanol gasses between free space and a unit cell of ZIF-8 (see Table S1 and Table S2 in Supplement 1, which are based on the gas adsorption analysis and data calculation for ZIF-8). In Fig. 3, a unit cell of ZIF-8 is surrounded by 26 virtual cubic unit cell volumes containing an ideal gas. The cubic unit cell parameter for the virtual and ZIF-8-unit cells is 1.6992 nm. The ZIF-8-unit cell volume consists of 49% scaffolding (metal-centers and organic linkers) and 51% empty space in the pore that is available to guest molecules.

For the case of an ideal gas at one atmosphere of gas pressure and 273.15 K (STP) surrounding the ZIF-8-unit cell, each of the surrounding 26 virtual cubic unit cells contains 0.131877 molecule of an ideal gas. Thus, a total of approximately 3.43 ideal gas molecules occupy the 26 virtual unit cells, a calculation that is accurate for any ideal gas at STP. In contradistinction, at equilibrium,

Optics EXPRESS

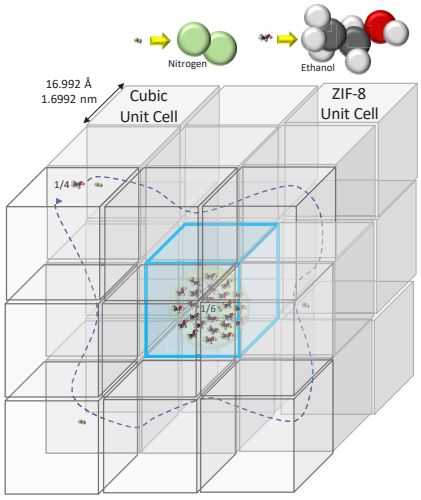

Fig. 3. A schematic drawing of a ZIF-8-unit cell containing guest molecules surrounded by 26 virtual unit cell cubic volumes of space containing gas molecules at equilibrium.

the ZIF-8-unit cell pore contains an average of 0.16 ideal gas molecules of nitrogen, according to published measured nitrogen gas adsorption isotherm data recorded at room temperature. The ratio of the amount of nitrogen gas molecules inside the ZIF-8 pores to those in a virtual unit cell at equilibrium is 0.16/0.12088 or 1.324 (Table S1). Therefore, the nitrogen molecule concentration enhancement factor for ZIF-8 at room temperature is 1.324, just somewhat larger than a value of 1, which represents a minimal concentration enhancement factor.

We can conclude that at STP or ambient conditions, nitrogen gas is a minor spectator interferent and it will not be necessary to include nitrogen molecules in RI calculations. On the other hand, 23 ethanol molecules occupy one ZIF-8 pore (saturation) at 0.079 atmospheres of ethanol gas at room temperature (ethanol saturation gas pressure), far less than one atmosphere of the partial pressure of ethanol gas at room temperature. This is because, at ethanol gas pressures above 0.079 atmosphere at room temperature, ethanol gas condenses to ethanol liquid. An ethanol gas pressure of 0.079 atmosphere at room temperature is equivalent to an average of 0.2483 ethanol molecules distributed over 26 virtual unit cells surrounding one ZIF-8-unit cell, or an average of 0.00955 ethanol gas molecule per one virtual unit cell.

The ratio of the amount of room-temperature ethanol gas molecules inside the ZIF-8 pores to those in a virtual unit cell at equilibrium is 23/0.00955 or 2408.4. Therefore, the ethanol molecule concentration enhancement factor for ZIF-8 at room temperature is 2408.4 for an ethanol partial pressure of 0.079 atmosphere, significantly larger than the same value for nitrogen molecules (1.324) at STP. We can conclude that at room temperature, ethanol gas molecules are the major adsorbate guests in ZIF-8 and will dominate the subsequent RI calculations. The graph in Fig. 4(a) includes a plot of the adsorption isotherm of ethanol in the MOF material ZIF-8. The data points were previously published by other researchers [4] as ethanol uptake in mmol/g versus pressure of ethanol gas (Table S4 - Table S9).

We have recast the data points with additional corresponding axes for the dependent and independent variables. Importantly, a microscopic visualization of the adsorption isotherm curve is formed by plotting the data as the number of adsorbed ethanol molecules per unit cell of ZIF-8 versus the number of molecules of ethanol in an equivalent ZIF-8-unit cell virtual volume under conditions of equilibrium. More importantly, for this research, the adsorption isotherm curve for

Optics EXPRESS

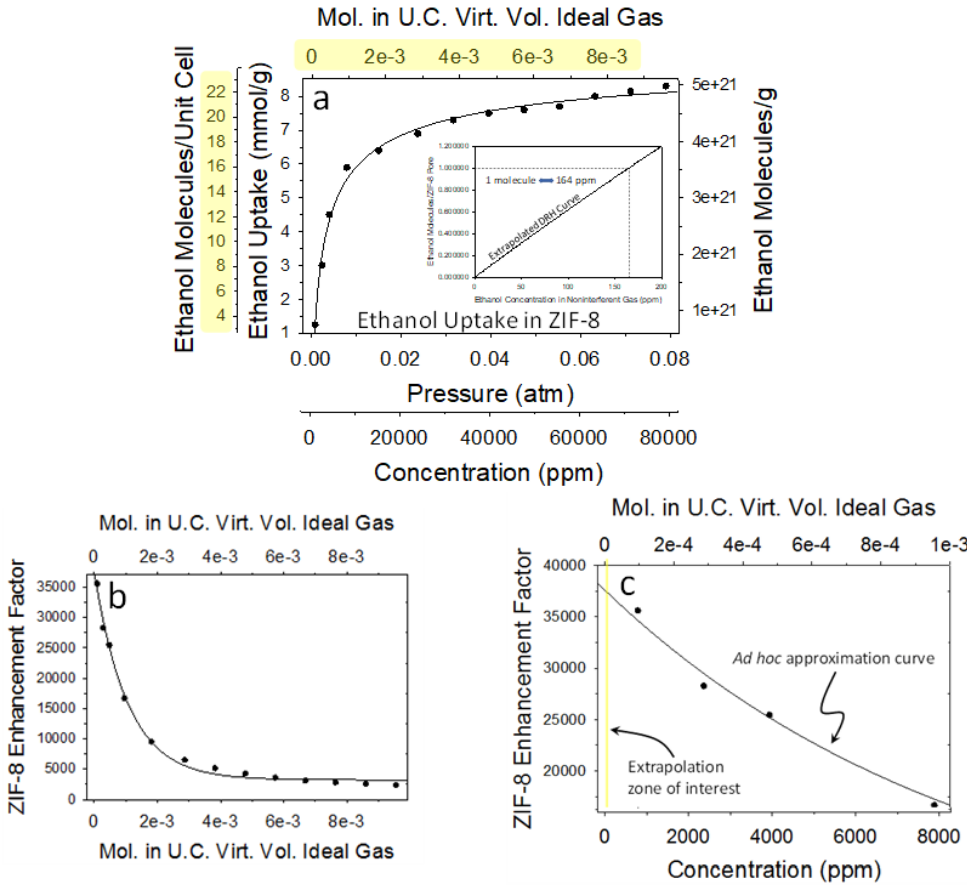

Fig. 4. (a) A graph of the uptake amount of ethanol guest molecules by ZIF-8 as a function of the pressure or equivalent concentration of ethanol molecules in the surrounding space volume (Vol), (b) a graph of a fitted solid curve mapping the ZIF-8 enhancement factor for ethanol as a function of pressure, and (c) a graph containing a plot of four data points from the ethanol adsorption isotherm in Fig. 4(a) and a plot of a fitted solid curve mapping the ZIF-8 enhancement factor for ethanol as a function of the concentration of ethanol in air.

ethanol is formed by plotting the relationship of the number of adsorbed ethanol molecules per unit cell of ZIF-8 versus the concentration of ethanol molecules in the surrounding environment.

We assumed ideal gas behavior for air (the diluent) and ethanol (the analyte) in the surrounding environment, and that the ambient air molecules afford a very small perturbation to the physicochemical adsorption process for ethanol. To proceed with a theoretical treatment of the changes in the RI's of guest/host MOF-based systems, it is necessary to fit the available adsorption isotherm data for any adsorption-analyte using a reasonable mathematical construct and use a fitted curve to extrapolate to very low, ppm-level, guest concentrations, *vide infra*.

The uptake of VOC molecules by ZIF-8 crystals is also critical for sensing performance and the ambient air molecules afford a very small perturbation to the physicochemical adsorption process for ethanol. This assumption is warranted given the comparison of the established adsorption isotherms for nitrogen versus ethanol in ZIF-8. The low selectivity of styrene, for example, can be attributable to the fact that the styrene molecule is too bulky to enter a ZIF-8 cage due to the cage's narrow aperture size.

Optics EXPRESS

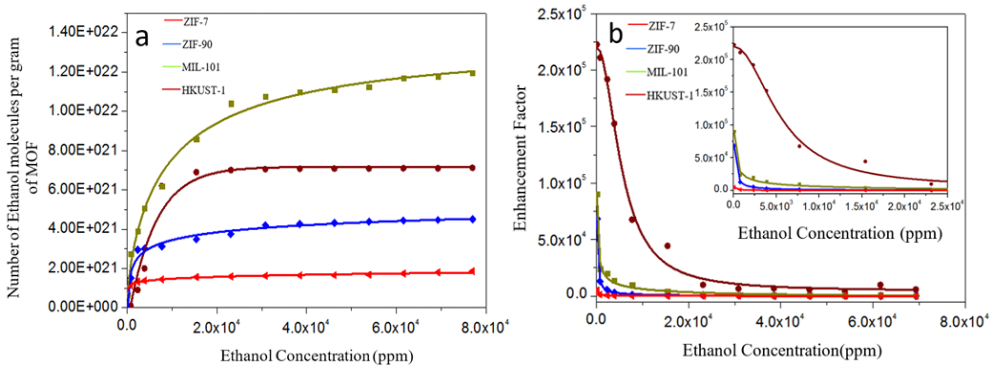

Fig. 5. (a) A graph of the uptake amount of ethanol guest molecules by ZIF-7, ZIF-90, MIL-101(Cr), and HKUST-1 as a function of the concentration of ethanol molecules in the surrounding space volume and (b) a graph of a fitted solid curve mapping estimations of the enhancement factors for the mentioned MOFs at room temperature.

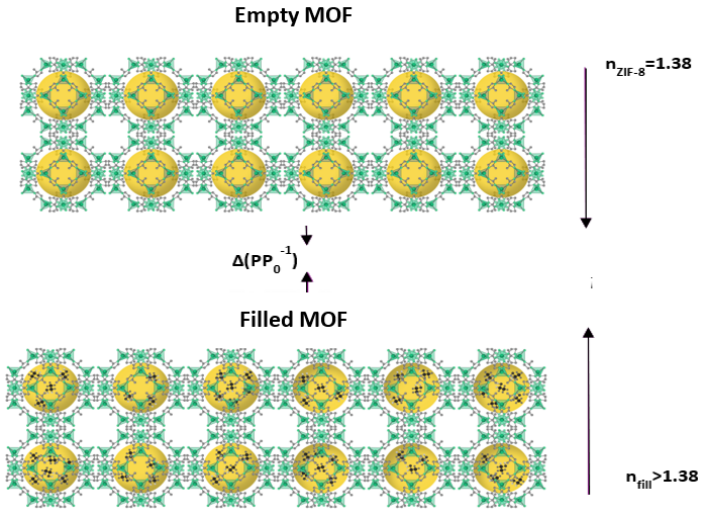

Fig. 6. The RI of a MOF as a function of adsorbate relative pressure based on the Lorentz–Lorentz, Maxwell–Ga equations. As an example, the refractive index values for ZIF-8 at a wavelength of 633 nm are presented.

Similarly, other VOC molecules such as tert-butanol are also too large to penetrate ZIF-8s' cage. The detection limits of primary alcohols are determined by the carbon number (or length) of the alkyl groups within the molecules, which increases in the following order: methanol, ethanol, propanol, butanol, pentanol, and hexanol. This phenomenon could be explained reasonably by increasing the hydrophobicity of the primary alcohols by extending their linear alkyl groups.

Furthermore, the typical type III water adsorption isotherm is observed with relatively low uptake at nearly saturated vapor pressures, which is related to ZIF-8's strong hydrophobic properties. The lack of hysteresis in the adsorption and desorption branches of alcohol sorption isotherms enables easy removal of deposited alcohols, which is advantageous for reversible sensing [35]. Under conditions of high temperatures and low partial pressures, ethanol also can be considered as an ideal gas that obeys the ideal gas equation of $PV = nk_BT$, where P and V are the pressure (pascal) and uptake volume (liter) by the gas, respectively. The variable n in

Optics EXPRESS

the ideal gas equation is the number of molecules in the gas, and k_B is Boltzmann's constant (1.38×10^{-23} J/K).

Consequently, we estimated the enhancement factor by taking the ratio of the number of VOC guests in the ZIF-8-unit cell (which is a smaller volume than the total volume of a unit cell) over the number of VOCs in a virtual ideal gas volume equal to the total volume of its cubic space group (4900 Å^3 for ZIF-8). Figure 4(b) and 4 (c) exhibit the data points from the ethanol adsorption isotherm and a plot of a fitted solid curve mapping the ZIF-8 enhancement factor for ethanol as a function of the pressure or concentration of ethanol in air. The lower end of the ethanol concentration range reveals large concentration enhancement factors (15000-35000) for ethanol molecules by ZIF-8.

The solid fitted curve, extrapolated to very low concentrations, shows a rapid increase in the ethanol concentration enhancement factors to values greater than 35000. The ability of ZIF-8 to concentrate molecules like ethanol in its pores, especially at very low analyte concentrations in an ambient environment, is a requirement of other MOFs for similarly concentrating and sensing ppm- and ppb-levels of analyte molecules in the same ambient environment. Thus, a concentration enhancement factor of approximately 40000 or greater should be considered a requirement when selecting a MOF for sensing analytes present at low ppm concentrations in an ambient environment. The variability of the general hyperbola shape for adsorption isotherms indicates that guest molecule concentration enhancement factors vary strongly with guest molecule and guest molecule loading.

2.1.2. Ethanol adsorption capacities in ZIF-7, HKUST-1, MIL-101(Cr), ZIF-90 at room temperature

We also calculated the number of ethanol molecules adsorbed per gram and unit cell volume of ZIF-7, ZIF-90, HKUST, and MIL-101(Cr) based on their adsorption isotherms extracted from the literature, as we can see in Fig. 5(a), Table S2 – Table S5 and Table S9 – Table S20. Water cannot be effectively adsorbed by ZIF-7 due to its hydrophobic nature, which is like that of ZIF-8. However, due to the presence of the hydrophilic carboxaldehyde group in the framework of ZIF-90, a substantial uptake of water was seen at higher relative partial pressures. MOFs exhibit variable selectivity upon loading of VOCs and water vapor because of the changes in the surface hydrophobicity, structural flexibility, and analyte physical properties. ZIF-7 has triclinic symmetry ($a = 23.948(6)$ Å, $b = 21.354(6)$ Å, $c = 16.349(4)$ Å, $\alpha = 90.28(2)°$, $\beta = 93.28(2)°$, $\gamma = 108.41(1)$) with a relatively large unit cell volume of $V = 7917(3)$ Å^3 [48]. MIL-101(Cr) is a MOF with a high porosity that has a zeotype cubic cell volume of 702000 Å^3 with a very large pore size and surface area, giving it the best characteristics when compared to other MOFs. Unit cell density and weight of MIL-101(Cr) are around 0.46 g/cm^3 and 3220×10^{-22} g, respectively [49,50].

HKUST-1 is water unstable, although it can maintain structural integrity in the presence of small amounts of water. The unit-cell volume of HKUST-1 is roughly 18213 Å^3 with 12 molecules per unit cell [51]. Although the ZIF-90 and ZIF-8 have the same space group and cubic framework, they have different substituents on the imidazolate ring. The unit cell volume of ZIF-90 is around 5152 Å^3 [52–54] which is 247 Å^3 larger than ZIF-8. According to Fig. 5(b), employing MOFs increased the number of adsorbed ethanol molecules at low pressure (0.000079 atmospheres) by up to 40000, 10000, 70000, 90000, and 222000 for ZIF-8, ZIF-7, ZIF-90, MIL-101(Cr), and HKUST-1, respectively. These values decreased to 371, 202, 1399, 1054, and 67636, respectively at the pressure of 0.0079 atmosphere, which is roughly 7700 ppm. These VOC adsorption curves at low pressure indicate a significant attractive interaction of gas to the interiors of the MOF pores.

Optics EXPRESS

2.2. Refractive index change

A successful optical-MOF sensor requires sufficient sensitivity for detecting VOC analyte molecules in the ambient environment at ppm-level concentrations. Once the sensitivity metric is met, the second requirement is high selectivity for the target VOC analyte molecule over interferent molecules, which generate incorrect results. The calculations below provide accurate quantification for metering the refractive index of guest-host systems. The guest-host system consists of VOC analyte molecule guests and a MOF single crystal host. Specifically, the change in the RI of the guest-host system is metered and related to the VOC material identity and the guest concentrations [55,56]. The need for a very high-resolution measurement of a gas RI, which must be achieved within a very narrow band of optical frequencies, is perhaps one of the reasons for the lack of interest in dispersion-based gas sensing. However, the RI of a gas varies fast at a frequency near the resonance frequency, while these changes are usually small at concentrations of interest, especially when the guest gas molecules are in a low concentration. [41,57–59].

2.2.1. Refractive index change calculation for MOF gas system

Ellipsometry is a technique for determining the change in the light polarization caused by specular reflection. The quantity absorbed is determined by detecting the change in optical characteristics of a porous material in ellipsometry porosimeter (EP) (Fig. 6). The refractive index (n) of the film increases as the pores gradually fill and empty space is replaced with adsorbate gas molecules. The ratio of the reflected p- and s-polarized light, often at varying wavelengths in the visible range, yields the two ellipsometry characteristics. By creating an optical model from the raw data, the change in RI at each partial pressure may be derived [60–62].

Several effective approximations can be utilized to obtain the adsorbate volume fraction from the RI change at different partial pressures. The Lorentz–Lorentz, Maxwell–Ga, and Bruggeman EMA equations are commonly applied to process EP data. Instead of charting the RI, these EMAs allow plotting the quantity adsorbed as a function of relative pressure. It is common practice to plot the RI at 633 nm, the working wavelength of helium–neon (HeNe) laser ellipsometers. Two forms of porosity can be specified for any porous material: open porosity and closed porosity. These can be achieved by adsorption-desorption and the solid-phase embedded methods, respectively. According to the Lorentz-Lorenz equations, the relative dielectric permittivity of a heterogeneous material can be determined by the permittivity of the material skeleton and that of the materials that fill the porosity (Eq. (1) to Eq. (3)). V_p is the filled pore volume. V_p is a function of the phase that fills the porosity and demonstrates the open porosity with dielectric permittivity ε_p. n is the index of refraction of the gas/MOF system at any stage of loading and n_p is the refractive index of the adsorbed material (for example, ethanol guest molecules, which form a 2-dimentional liquid inside the pores). n_s is the refractive index of the MOF's framework without considering the empty part that will be filled with air prior to gas adsorption.

$$\varepsilon = V_p \varepsilon p + 1 - V_p \varepsilon s \tag{1}$$

$$\frac{\varepsilon - 1}{\varepsilon + 2} = V_p \frac{\varepsilon_p^2 - 1}{\varepsilon_p^2 + 2} + (1 - V_p) \frac{\varepsilon_s^2 - 1}{\varepsilon_s^2 + 2} \tag{2}$$

$$\frac{n^2 - 1}{n^2 + 2} = V_p \frac{n_p^2 - 1}{n_p^2 + 2} + (1 - V_p) \frac{n_s^2 - 1}{n_s^2 + 2} \tag{3}$$

The film porosity V_p is calculated using the Lorentz–Lorenz equation ((Eq. (4)), where B is the polarizability of a unit of volume, N_i and α_i are the number of molecules and the molecular polarizability of the material components, respectively. n_{MOF} and n_s are the film's and skeleton's

Optics EXPRESS

refractive indices, respectively. The volume fraction filled by the gas molecules is proportional to the concentration of gas molecules adsorbed inside the MOF:

$$B = \sum N_i \alpha_i = \frac{3(n^2-1)}{4\pi(n^2+2)} \tag{4}$$

$$V_p = 1 - \frac{\frac{n_{MOF}^2-1}{n_{MOF}^2+2}}{\frac{n_s^2-1}{n_s^2+2}} \tag{5}$$

By substituting Eq. (4) for V_p, we have the final formula:

$$\frac{n_{fill}^2-1}{n_{fill}^2+2} = V\frac{n_{ads}^2-1}{n_{ads}^2+2} + (V_p - V)\frac{n_u^2-1}{n_u^2+2} + (1-V_p)\frac{n_s^2-1}{n_s^2+2} \tag{6}$$

$$V = \frac{\frac{n_{fill}^2-1}{n_{fill}^2+2} - \frac{n_{MOF}^2-1}{n_{MOF}^2+2}}{\frac{n_{ads}^2-1}{n_{ads}^2+2}} \tag{7}$$

$$n_{fill} = \sqrt{\frac{2(V\frac{n_{ads}^2-1}{n_{ads}^2+2} + \frac{n_{MOF}^2-1}{n_{MOF}^2+2}) + 1}{1 - (V\frac{n_{ads}^2-1}{n_{ads}^2+2} + \frac{n_{MOF}^2-1}{n_{MOF}^2+2})}} \tag{8}$$

V (occupied volume fraction by mixed gases) $= V_1 + V_2 + V_3 + \ldots$

An EMA would need three components (Eq. (6)–Eq. (8)) to describe porous materials with partially filled pores: the volumes taken up by (1) the framework, (2) the absorbate, and (3) the empty space. Measurements at extreme partial pressures ($P\,P_0{}^{-1} = 0$ and $P\,P_0{}^{-1} \approx 1$) are utilized to simplify this problem. The n and n_s are equal when the pores are empty ($PP_0{}^{-1} = 0$). At intermediate levels of pore filling, a basic two-component EMA is utilized, with the "empty" and "full" materials being treated separately. The volume of adsorbate is calculated by multiplying the volume fraction of "loaded" material by the total volume of the adsorbent at each partial pressure. The latter can be derived from ellipsometry data or by other means [39,41,57]. By expanding Eq. (6), we achieve the below formula for gas mixtures:

$$V_1\frac{n_{ads1}^2-1}{n_{ads1}^2+2} + V_2\frac{n_{ads2}^2-1}{n_{ads2}^2+2} + V_3\frac{n_{ads3}^2-1}{n_{ads3}^2+2} + \ldots = \frac{n_{fill}^2-1}{n_{fill}^2+2} - \frac{n_{MOF}^2-1}{n_{MOF}^2+2} \tag{9}$$

2.2.2. Refractive index change of ZIF-8 for ethanol adsorption

MOFs' refractive index shift following guest adsorption also provides intriguing optical sensing possibilities. Férey and coworkers [40] were the first to demonstrate the magnitude of this phenomenon using spin-coated MIL-101(Cr) thin films on silicon. When the film was exposed to several volatile compounds, spectroscopic ellipsometry revealed changes in the refractive index of up to 30%. The refractive index shift must be converted into a quantifiable optical signal before this effect can be used in practice. Mesoscopic structuring of MOFs as photonic etalons, Bragg stacks, and two-dimensional or three-dimensional photonic crystals can be used in a variety of techniques to attain this purpose. These structures are characterized by regularly repeated sections of high and low refractive index materials. Photonic behavior produces distinguishable colors through interference and diffraction when the periodicity is close to half the wavelength (i.e., 200–400 nm for the visible range). Color changes caused by analyte adsorption are commonly

Optics EXPRESS

monitored during the readout. We can determine the volume of an ethanol molecule by using the liquid's density (0.78808 g/ml), which is determined to be about 95.5 Å^3. Refractive index values for ZIF-8 at a wavelength of 633 nm is 1.38 and for ethanol as an adsorbed molecule is 1.361. The volume fraction occupied by one molecule of ethanol can be achieved by dividing 95.5 Å^3 into 2500 Å^3 (ZIF-8-unit cell volume). According to Eq. (7), when the pores are empty ($P\,P_0{}^{-1} = 0$), n_{fill} (RI of MOF-based systems after gas adsorption) is equal to n_{MOF} (RI of MOF).

It might be difficult to estimate the number of adsorbed molecules at low relative pressures of alcohol if simply done by applying their adsorption isotherms. For the aforementioned reasons, we must find suitable adsorption isotherm models to compute the number of adsorbed molecules at low pressures. The Langmuir adsorption isotherm, which was first created to explain gas solid-phase adsorption onto activated carbon, has long been used to compare and evaluate the performance of various bio-sorbents. This empirical model is based on monolayer adsorption, with adsorption occurring only at a limited number of specified localized sites without lateral interaction between the adsorbed molecules, even in nearby places. The linearized form of the Langmuir isotherm model can be applied to define the number of ethanol molecules adsorbed in ZIF-8, particularly at low pressures. To illustrate the mentioned model, Eq. (10) and Eq. (11) are simplified. In these equations, P and P_0 represent the relative and saturation pressures, respectively. Moreover, θ is characterized as the portion of the total volume that the gas molecules occupy [63]. K_0 and ε are the Langmuir constant and binding energy, respectively. Based on Eq. (11), we completed the calculation of the RI change for ZIF-8 at low concentrations of ethanol ranging from 1 ppm to 77 ppm.

$$\theta = \frac{KP}{1 + KP} \tag{10}$$

$$K = \frac{1}{P_0} e^{\frac{-\varepsilon}{K_0 T}} \tag{11}$$

Table 2 and Fig. 7(a) summarize the refractive index change of ZIF-8 due to ethanol adsorption ranging from 1 ppm to 100 ppm and, Table 3 and Fig. 7(b) from 100 ppm to 77000 ppm. In Table 2 and Table 3, Refractive Index Change (Δn) is defined as the negative of the difference in the index refraction of ZIF-8 before (the RI value for ZIF-8 at a wavelength of 633 nm is 1.38) and after ethanol exposure (n_{fill}, Eq. (8)). As we can see, Δn varied from 0.000001 to 0.396 for the corresponding changes in ethanol concentrations of 1 to 77000 ppm. In addition, the percentage change of the index of refraction (Δn%) ranges from 0.00009% to 28.6% for the same range of ethanol concentrations. Also, the slope of the RI versus adsorbate concentration curve (Δn% versus ethanol concentration) at low concentrations of ethanol is greater than at high ethanol concentrations, which is a common distinguishing feature of adsorption isotherms (Fig. 7(a)). A typical adsorption isotherm has an initial convex shape, indicating that a large amount of adsorption occurs at low partial pressures. A large change in the number of adsorbed ethanol molecules at low ambient ethanol concentrations occurs because there is a large available space in empty ZIF-8, and as discussed in Eq. (8), results in a large change in the index of refraction. The slope of the RI versus ethanol concentration curve in Fig. 7(b) is very low, below ethanol concentrations of 50 ppm. We believe this is explained by the use of the specific Langmuir Eq. (10) and Eq. (11).

Table 2. The percentage change in the Index of Refraction (Δn%) and Refractive Index Change (Δn) calculations for ZIF-8 based on the adsorption isotherms of ethanol.

ppm	770	2310	3850	7700	15400	23100	30800	38500	46200	53900	61600	69300	77000
Δn	0.004	0.13	0.18	0.27	0.29	0.32	0.34	0.355	0.361	0.366	0.381	0.391	0.396
Δn%	0.72%	9.4%	13%	19%	21%	23%	24%	25%	26%	26.5%	27.6%	28.3%	28.6%

Optics EXPRESS

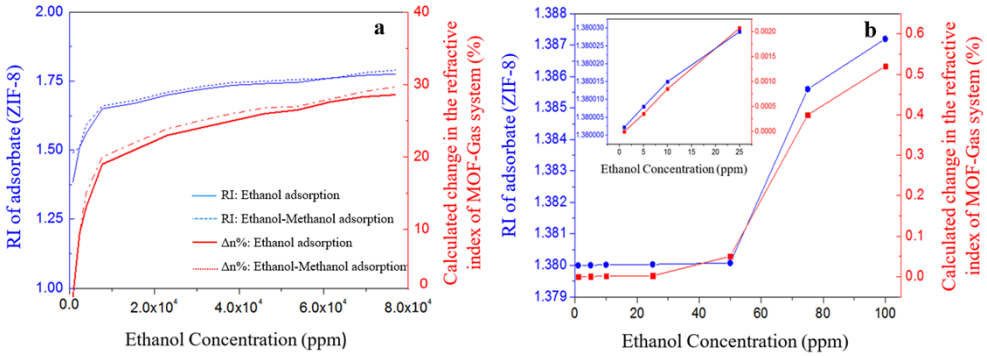

Fig. 7. Refractive index change of ZIF-8 upon ethanol exposure at (a) high and (b) low concentrations of ethanol.

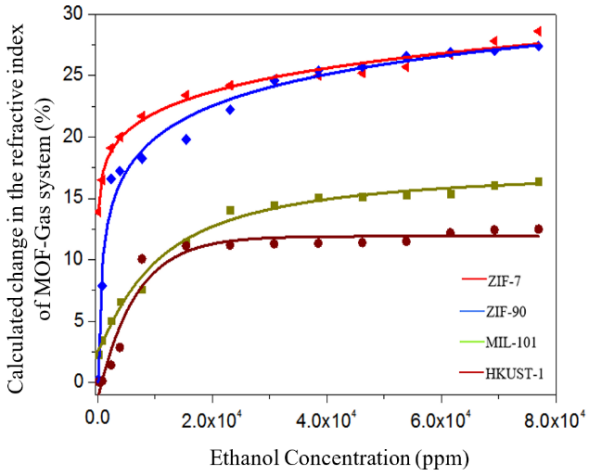

Fig. 8. Percentage change in the RI of ZIF-7, HKUST-1, MIL-101(Cr), and ZIF-90 as a function of various concentrations of ethanol at room temperature.

Table 3. The percentage change in the Index of Refraction (Δn%) and Refractive Index Change (Δn) calculations for ZIF-8 at low concentrations of ethanol characterized by the linear Langmuir adsorption model.

Concentration	1ppm	5ppm	10ppm	25ppm	50ppm	75ppm	100ppm
Δn(e-4)	0.01	0.06	0.13	0.30	7.78	56	72
Δn%	9e-5	5e-4	0.001	0.002	0.05	0.4	0.52

Jieyun Wu, et. al. [64] created an in-line fiber Mach-Zehnder interferometer to control the co-propagating cladding mode LP08 in nano-porous ZIF-8. Density functional theory (DFT) calculations and experimental interfering spectra for vapor-MOF interactions revealed that ZIF-8's large surface area and high porosity resulted in large refractive index changes (RI changes from initial 1.216 to 1.499). As a result, ethanol adsorption inside ZIF-8 with the lowest desorption energy caused the greatest Δn% of ≈ 24% [64]. According to our calculations in Table 2, Δn% in the saturation area is in the range of 26% to 28%, which is very close to the mentioned experimental results (Δn% of ≈ 24%).

Optics EXPRESS

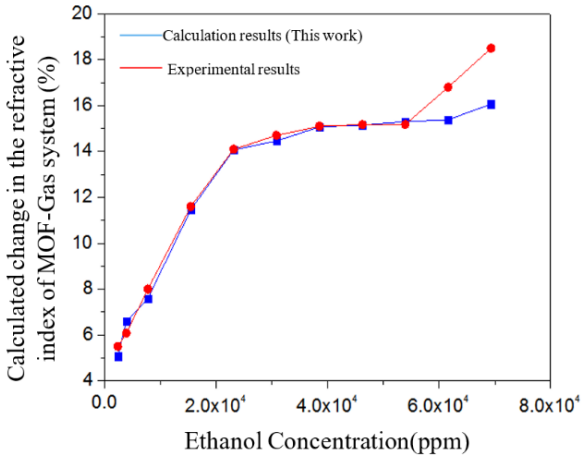

Fig. 9. Percentage change in the refractive index of MIL-101(Cr) upon exposure to C_2H_6O, based on the calculations (this study) and experimental data.

2.2.3. Refractive index change of ZIF-8 for gas mixtures adsorption

The RI variation of two different gases, including the constant concentration of methanol (8000 ppm) with varying concentrations of ethanol, is calculated using Eq. (8) (by expanding Eq. (6)) to acquire a better understanding of the computation, as given in Table 4. The molecular weight of methanol is 32.04 g/mol and its density is 0.78 g/ml with an RI of 1.33 and a volume of 60 A^3. In 8000 ppm methanol, 0.31 mmol/g will be adsorbed inside ZIF-8 which is equal to 1.86×10^{20} molecules in one gram of ZIF-8. More details regarding the calculations are available in the Supplement 1 of this paper. The change in the RI for the mixture of gases is a bit larger than the single gas adsorption, likely caused by the difference in the indices of refraction of ethanol and methanol.

Table 4. Δn% and Δn calculations for ZIF-8 based on the C_2H_6O adsorption isotherm at room temperature in the case of 8000 ppm of CH_4O.

ppm	770	2310	3850	7700	15400	23100	30800	38500	46200	53900	61600	69300	77000
Δn	0.11	0.13	0.21	0.28	0.30	0.33	0.35	0.365	0.37	0.376	0.39	0.4	0.41
Δn%	7.9%	9.4%	15%	20%	22%	23.9%	25%	26%	26.8%	27%	28%	29%	29.7%

2.2.4. Refractive index change of ZIF-7, HKUST-1, MIL-101(Cr) and ZIF-90 for ethanol adsorption

Table 5 and Fig. 8 demonstrate the change in the index of refraction for ZIF-7, HKUST-1 MIL-101(Cr), and ZIF-90, upon ethanol adsorption ranging from 77 ppm to 77000 ppm. The Δn% changed from 13.9% to 28.6%, 0.08% to 12.5%, 2.3% to 16.38%, 0.23% to 27.4%, and 0.4% to 28.9% for ZIF-7, HKUST-1, MIL-101(Cr), ZIF-90, and ZIF-8, respectively, upon exposure to 77 ppm to 77000 ppm of ethanol gas.

The RI of HKUST-1 and MIL-101(Cr) before ethanol adsorption at room temperature and 750 nm is 1.39 and 1.3, respectively. Furthermore, at 1,131 nm, the index of refraction of ZIF-7 and ZIF-90 is 1.15 and 1.26, respectively. The mentioned primary RI of the MOFs and a graph of the uptake amount of ethanol guest molecules by ZIF-7, ZIF-90, MIL-101(Cr), and HKUST-1 (Fig. 5) are used to calculate Δn and Δn% for other MOFs, by employing Eq. (8).

Optics EXPRESS

Table 5. Δn% and Δn calculations for ZIF-7, HKUST-1, MIL-101(Cr) and ZIF-90 because of responding to different concentrations of C_2H_6O

ppm	77	770	2310	3850	7700	15400	23100	30800	38500	46200	53900	61600	69300	77000
Δn/ZIF-7	0.16	0.19	0.22	0.239	0.25	0.27	0.279	0.285	0.288	0.29	0.296	0.308	0.32	0.33
Δn%/ZIF-7	13.9	16.5	19.1	20	21.7	23.4	24.2	24.7	25	25.2	25.7	26.7	27.8	28.6
Δn/HKUST-1	0.0006	0.002	0.02	0.04	0.14	0.155	0.157	0.157	0.158	0.159	0.16	0.17	0.173	1.74
Δn%/HKUST-1	0.08	0.14	1.43	2.87	10.07	11.15	11.2	11.3	11.36	11.4	11.5	12.2	12.44	12.5
Δn/ MIL-101(Cr)	0.03	0.04	0.066	0.086	0.1	0.149	0.183	0.188	0.196	0.197	0.199	0.2	0.209	0.213
Δn%/ MIL-101(Cr)	2.3	3.46	5.07	6.6	7.6	11.46	14.07	14.46	15.07	15.15	15.3	15.38	16.07	16.38
Δn/ZIF-90	0.003	0.1	0.21	0.217	0.23	0.25	0.28	0.31	0.32	0.33	0.336	0.341	0.343	0.346
Δn%/ZIF-90	0.23	7.9	16.6	17.22	18.25	19.8	22.22	24.6	25.39	25.7	26.6	26.9	27	27.4

As shown in Table 5, at the lowest measured concentration (77 ppm), ZIF-7 and HKUST-1 had the highest and lowest index refraction changes, respectively. Furthermore, at high vapor pressures near the saturation area, ZIF-90 and ZIF-7 exhibit very similar amounts for Δn% (28.6% and 27.4%). Analyzing Fig. 8 demonstrates that at low concentrations of ethanol, the slope of the graph is sharp for ZIF-90 and ZIF-7, and the slope is relatively flat for the other MOFs (HKUST and MIL-101(Cr)). These observations can be explained by the low ethanol adsorption inside ZIF-7 and MIL-101(Cr) at low concentrations as well as the fact that the starting pressure for gas adsorption differs between them. Using different MOFs with different enhancement factors for gases could be a good way to build gas sensors and improve their selectivity.

We found evidence for our RI change computations, which included the evolution of the RI of one deposition of MIL-101(Cr) film upon ethanol adsorption. This paper and its calculations can serve as a starting point to develop further calculations for other MOFs and mesoporous materials based on our current data. MIL-101(Cr) is a highly porous MOF capable of large adsorptions on films that can be studied by environmental ellipsometry porosity. At $P/P_0 = 0$, a freshly cast thin film had a thickness of 70.1 nm and a low refractive index (1.11) [65]. The desorption of ethanol molecules inside the pores of MIL-101(Cr) showed a hysteresis loop due to MOF cage windows acting as a restriction to water desorption. As we can see in Fig. 9, all our calculations for the changes in the index of refraction of MIL-101(Cr) due to ethanol adsorption, excluding the saturation area, are close to the previously reported experimental data, which points out the high accuracy of our calculations. The MIL-101(Cr) film adsorbed almost no water molecules at low water vapor pressure, emphasizing the hydrophobic pore character of the terephthalate-based MOF. However, after water desorption at high vapor pressure, near the saturation zone, the refractive index did not return to its primary value, showing that a small amount of water, either chemisorbed or coordinated, remained trapped in the film. This could be the explanation for the difference between the experimental and computational data (found in this paper) at high ethanol gas pressures [65,66].

According to the review of the literature, there are three basic options for gas detection using MOFs adsorption: (1) Electrical sensing by measuring resistivity and conductivity as electrical characteristics; (2) Mass weighting using a micro-electro-mechanical system; (3) Detecting variations in the frequency-based optical properties (i.e., wavelength and the index of refraction). These characteristics can differ depending on the gas species and concentrations, which the former can aid in increasing detection accuracy. The photonic micro-ring resonator (MRR) resonant wavelength is highly influenced by variations in a MOF's RI caused by gas adsorption. The sensor's sensitivity is described as wavelength shift ($\Delta\lambda$) divided by gas concentration *(C),* $\frac{\Delta\lambda}{C}$. When compared to gravimetric and electrical sensing approaches, the third approach has the potential to further reduce VOC detection limitations. It also can be utilized as a versatile tool to investigate the optical characteristics of MOFs. Undoubtedly, our estimations for changes in the

Optics EXPRESS

index of refraction and enhancement factors discussed above can be useful in determining the benefits and drawbacks of various MOFs for several applications [35,38,67,68].

3. Conclusion

In summary, we demonstrated a proof-of-concept for VOC detection by calculating one frequency-dependent optical property of MOF-based sensors, the refractive index. We used the Lorentz–Lorentz, Maxwell–Ga, and Bruggeman effective medium approximations equations to process ellipsometry porosimeter data. Except for the saturation zone, all our calculations of the changes in the index of refraction for MIL-101(Cr) due to ethanol adsorption were close to the previously reported experimental data, demonstrating the high accuracy of our calculations for the other studied MOFs, as well. The small differences between theoretical and experimental data can be due to trapping water molecules in the MIL-101(Cr) film at high water vapor pressures without returning to their initial RI value, even after water desorption. Additionally, our $\Delta n\%$ calculations of ZIF-8 upon exposure to ethanol in the saturation zone in the range of 26% to 28%, are very close to Wu's experimental results (26%). We also computed the enhancement factors of ZIF-7, HKUST-1, MIL-101(Cr), ZIF-90, and ZIF-8 upon exposure to ethanol based on the periodic structures such as unit cell volume and the number of atoms per unit cell. The results exhibit the highest concentration factor of 225000 for HKUST-1 and the lowest value of 10000 for ZIF-7 at low pressures, which demonstrates the MOF-based sensor's selective detection behavior upon exposure to chemical vapors. The large change in the index of refraction of HKUST-1 at much smaller vapor pressures indicates that HKUST-1 may be superior to other MOFs in its potential for gas sensors and biosensors applications. As calculated in the graph's lower pressure region, ZIF-7 and HKUST-1 had the largest and smallest changes in the index of refraction for ethanol loading, respectively. This finding suggests that the selectivity of MOFs towards gases is an effective way to improve gas sensor specificity. This level of selectivity can be obtained by effectively incorporating the desired functionality into the synthesis process. Furthermore, we plan in the future to solve the mapping problem (selectivity) by studying the interaction of polarized light with guests in oriented MOF single crystals. The presented platform can open an avenue toward designing highly sensitive breath analyzers using MOF-coated devices.

Funding. National Science Foundation (2027571); National Institute of Biomedical Imaging and Bioengineering (3U01HL152410-02S1).

Acknowledgments. Research was also partly sponsored by the Army Research Laboratory and was accomplished under Cooperative Agreement Number W911NF-21-2-0274. The views and conclusions contained in this document are those of the authors and should not be interpreted as representing the official policies, either expressed or implied, of the Army Research Office or the U.S. Government. The U.S. Government is authorized to reproduce and distribute reprints for Government purposes notwithstanding any copyright notation herein.

Disclosures. The authors declare no conflicts of interest.

Data availability. Data underlying the results presented in this paper are publicly available in the Supplement 1.

Supplemental document. See Supplement 1 for supporting content.

References

1. M. Bergaoui, M. Khalfaoui, A. Awadallah-F, and S. Al-Muhtaseb, "A review of the features and applications of ZIF-8 and its derivatives for separating CO_2 and isomers of C_3-and C_4-hydrocarbons," J. Nat. Gas Sci. Eng. **96**, 104289 (2021).
2. L. Li, X. Jiao, C. Xiuling, D. Lotsch, V. Bettina, and C. Li, "Facile fabrication of ultrathin metal–organic framework-coated monolayer colloidal crystals for highly efficient vapor sensing," Chem. Mater. **27**(22), 7601–7609 (2015).
3. V. Sánchez, P. Elvia, A. Knebel, L. Sánchez, M. Klumpp, C. Wöll, and R. Dittmeyer, "Studying ZIF-8 SURMOF Thin Films with a Langatate Crystal Microbalance: Single-Component Gas Adsorption Isotherms Measured at Elevated Temperatures and Pressures," Langmuir **36**(29), 8444–8450 (2020).
4. M. T. Huang, S. Wannapaiboon, K. Khaletskaya, and R. A. Fischer, "Engineering zeolitic-imidazolate framework (ZIF) thin film devices for selective detection of volatile organic compounds," Adv. Funct. Mater. **25**(28), 4470–4479 (2015).

Optics EXPRESS

5. S. Yue, C. Oh, A. Nandy, G. Terrones, and H. Kulik, "Effects of MOF linker rotation and functionalization on methane uptake and diffusion," Molecular Systems Design & Engineering, (2023).
6. H. Yuan, N. Li, W. Fan, H. Cai, and D. Zhao, "Metal-Organic Framework Based Gas Sensors," Adv. Sci. **9**(6), 2104374 (2022).
7. Y. Sun, Z. Zhao, K. Suematsu, W. Zhang, W. Zhang, S. Zhuiykov, K. Shimanoe, and J. Hu, "MOF-derived Au-NiO/In2O3 for selective and fast detection of toluene at ppb-level in high humid environments," Sens. Actuators, B **360**, 131631 (2022).
8. E. M. Gaspar, A. F. Lucena, J. D. da Costa, and H. C. das Neves, "Quantitative Analysis of Urine Vapor and Breath by Gas-Liquid Partition Chromatography," Proc. Natl. Acad. Sci. **68**(10), 2374–2376 (1971).
9. M. Phillips, "Method for the collection and assay of volatile organic compounds in breath," Anal. Biochem. **247**(2), 272–278 (1997).
10. D. Souvik, P. Saurabh, and M. Madhuchhanda, "Significance of Exhaled Breath Test in Clinical Diagnosis: A Special Focus on the Detection of Diabetes Mellitus," J. Med. Biol. Eng. **36**(5), 605–624 (2016).
11. J. D. Fenske and S. E. Paulson, "Human breath emissions of VOCs," Journal of the Air & Waste Management Assosiation **49**(5), 594–598 (1999).
12. A. Schütze, T. Baur, M. Leidinger, W. Reimringer, R. Jung, T. Conrad, and T. Sauerwald, "Highly sensitive and selective VOC sensor systems based on semiconductor gas sensors: how to?" Environments **4**(1), 20 (2017).
13. A. H. Jalal, F. Alam, S. Roychoudhury, Y. Umasankar, N. Pala, and S. Bhansali, "Prospects and challenges of volatile organic compound sensors in human healthcare," ACS Sens. **3**(7), 1246–1263 (2018).
14. K. Westphal, D. Dudzik, M. Waszczuk-Jankowska, B. Graff, K. Narkiewicz, and M. J. Markuszewski, "Common Strategies and Factors Affecting Off-Line Breath Sampling and Volatile Organic Compounds Analysis Using Thermal Desorption-Gas Chromatography-Mass Spectrometry (TD-GC-MS)," Metabolites **13**(1), 8 (2022).
15. A. Wehinger, A. Schmid, S. Mechtcheriakov, M. Ledochowski, C. Grabmer, G. A. Gastl, and A. Amann, "Lung cancer detection by proton transfer reaction mass-spectrometric analysis of human breath gas," Int. J. Mass Spectrom. **265**(1), 49–59 (2007).
16. K. H. Kim, S. A. Jahan, and E. Kabir, "A review of breath analysis for diagnosis of human health," Trends Anal. Chem. **33**, 1–8 (2012).
17. Z. Tang, Y. Liu, and Y. Duan, "Breath analysis: Technical developments and challenges in the monitoring of human exposure to volatile organic compounds," Journal of Chromatography B **1002**, 285–299 (2015).
18. W. Miekisch and J. K. chubert, "From highly sophisticated analytical techniques to life-saving diagnostics: Technical developments in breath Analysis," Trends Anal. Chem. **25**(7), 665–673 (2006).
19. S. M. Usman Ali, O. Nur, M. Willander, and B. Danielsson, "A fast and sensitive potentiometric glucose microsensor based on glucose oxidase coated ZnO nanowires grown on a thin silver wire," Sens. Actuators, B **145**(2), 869–874 (2010).
20. Z. Zhenyu, X. Zhang, J. Wang, L. Huiyu, Y. Sun, X. Hao, Y. Qin, B. Niu, and C. Li, "Washable and flexible gas sensor based on UiO-66-NH2 nanofibers membrane for highly detecting SO_2," Chem. Eng. J. **428**, 131720 (2022).
21. M. M. Mohseni, M. Jouyandeh, S. M. Sajadi, A. Hejna, S. Habibzadeh, A. Mohaddespour, N. Rabiee, H. Daneshgar, O. Akhavan, M. Asadnia, and M. Rabiee, "Metal-organic frameworks (MOF) based heat transfer: A comprehensive review," Chem. Eng. J. **449**, 137700 (2022).
22. D. N. Dybtsev, H. Chun, S. H. Yoon, D. Kim, and K. Kim, "Microporous Manganese Formate: A Simple Metal−Organic Porous Material with High Framework Stability and Highly Selective Gas Sorption Properties," J. Am. Chem. Soc. **126**(1), 32–33 (2004).
23. Y. Wang and D. Zhao, "Beyond equilibrium: metal–organic frameworks for molecular sieving and kinetic gas separation," Cryst. Growth Des. **17**(5), 2291–2308 (2017).
24. S. Ma, D. Sun, D. Yuan, X. S. Wang, and H. C. Zhou, "Preparation and Gas Adsorption Studies of Three Mesh-Adjustable Molecular Sieves with a Common Structure," J. Am. Chem. Soc. **131**(18), 6445–6451 (2009).
25. C. Zhu, R. E. Gerald, and J. Huang, "Micromachined Optical Fiber Sensors for Biomedical Applications," Biomedical Engineering Technologies **2393**, 367–414 (2022).
26. S. Radhakrishnan, M. Mathew, and C. S. Rout, "Microfluidic sensors based on two-dimensional materials for chemical and biological assessments," Mater. Adv. **3**(4), 1874–1904 (2022).
27. H. C. Ates, P. Q. Nguyen, L. Gonzalez-Macia, E. Morales-Narváez, F. Güder, J. J. Collins, and C. Dincer, "End-to-end design of wearable sensors," Nat. Rev. Mater. **7**(11), 887–907 (2022).
28. M. Khatib and H. Haick, "Sensors for Volatile Organic Compounds," ACS Nano **16**, 7080–7115 (2022).
29. Z. Z. Lu, R. Zhang, Y. Z. Li, Z. J. Guo, and H. G. Zheng, "Solvatochromic behavior of a nanotubular metal− organic framework for sensing small molecules," J. Am. Chem. Soc. **133**(12), 4172–4174 (2011).
30. D. Zhao, K. Yu, X. Han, Y. He, and B. Chen, "Recent progress on porous MOFs for process-efficient hydrocarbon separation, luminescent sensing, and information encryption," Chem. Commun. **58**(6), 747–770 (2022).
31. L. G. Qiu, Z. Qun, Y. Wu, W. Wang, T. Xu, and X. Jiang, "Facile synthesis of nanocrystals of a microporous metal–organic framework by an ultrasonic method and selective sensing of organoamines," Chem. Commun. **31**(31), 3642–3644 (2008).
32. X. Zou, G. Zhu, I. J. Hewitt, F. Sun, and S. Qiu, "Synthesis of a metal–organic framework film by direct conversion technique for VOCs sensing," Dalton Trans. **16**(16), 3009–3013 (2009).

Optics EXPRESS

33. C. Zhu, R. E. Gerald, and J. Huang, "Metal-organic Framework Materials Coupled to Optical Fibers for Chemical Sensing: A Review," IEEE Sens. J. **21**(18), 19647–19661 (2021).
34. S. Khan, S. Le Calvé, and D. Newport, "A review of optical interferometry techniques for VOC detection," Sens. Actuators, A **302**, 111782 (2020).
35. J. Wang, Y. Liu, G. Bleyer, E. S. Goerlitzer, S. Englisch, T. Przybilla, C. F. Mbah, M. Engel, E. Spiecker, I. Imaz, and D. Maspoch, "Coloration in Supraparticles Assembled from Polyhedral Metal-Organic Framework Particles," Angewandte Chemie International Edition **61**(16), e202117455 (2022).
36. L. E. Kreno, J. T. Hupp, and R. P. Van Duyne, "Metal− organic framework thin film for enhanced localized surface plasmon resonance gas sensing," Anal. Chem. **82**(19), 8042–8046 (2010).
37. M. L. Tietze, M. Obst, G. Arnauts, N. Wauteraerts, S. Rodríguez-Hermida, and R. Ameloot, "Parts-per-Million Detection of Volatile Organic Compounds via Surface Plasmon Polaritons and Nanometer-Thick Metal–Organic Framework Films," ACS Appl. Nano Mater. **5**(4), 5006–5016 (2022).
38. J. Tao, X. Wang, S. Tao, H. Cai, Y. Wang, T. Lin, D. Fu, L. L. Y. Ting, Y. Gu, and Z. Dan, "Hybrid photonic cavity with metal-organic framework coatings for the ultra-sensitive detection of volatile organic compounds with high immunity to humidity," Sci. Rep. **7**(1), 1–8 (2017).
39. T. Stassin, R. Verbeke, A. J. Cruz, S. Rodríguez-Hermida, I. Stassen, J. Marreiros, M. Krishtab, W. Dickmann, I. F. Egger, and Vankelecom, "Porosimeter for Thin Films of Metal–Organic Frameworks: A Comparison of Positron Annihilation Lifetime Spectroscopy and Adsorption-Based Methods," Adv. Mater. **33**(17), 2006993 (2021).
40. D. Aude, C. Boissière, D. Grosso, P. Horcajada, C. Serre, G. Férey, J. A. Galo, A. Soler-Illia, and C. Sanchez, "Adsorption properties in high optical quality nano ZIF-8 thin films with tunable thickness," J. Mater. Chem. **20**(36), 7676–7681 (2010).
41. Y. Shigeru, I. Kenji, H. Hosomi, and Y. Takai, "Comparison study of mesoporous thin films characterized by low-energy positron lifetime spectroscopy and flow-type ellipsometric porosimetry," in *JJAP Conference Proceedings 2nd Japan-China Joint Workshop on Positron Science*. The Japan Society of Applied Physics, 011205 (2014).
42. H. Kragh, "The Lorenz-Lorentz formula: Origin and early history," Substantia **2**(2), 7–18 (2018).
43. K. J. Kim, P. Lu, J. T. Culp, and P. R. Ohodnicki, "Metal–organic framework thin film coated optical fiber sensors: a novel waveguide-based chemical sensing platform," ACS Sens. **3**(2), 386–394 (2018).
44. O. Barash, W. Zhang, J. M. Halpern, Q. Hua, Y. Y. Pan, K. Haneen, K. Khoury, H. Liu, M. P. A. Davies, and H. Haick, "Differentiation between genetic mutations of breast cancer by breath volatolomics," Oncotarget **6**(42), 44864–44876 (2015).
45. A. Altieri, W. Garavello, C. Bosetti, S. Gallus, and C. L. Vecchia, "Alcohol consumption and risk of laryngeal cancer," Oral Oncology **41**(10), 956–965 (2005).
46. J. Gray, N. Evans, B. Taylor, J. Rizzo, and M. Walker, "State of the evidence: the connection between breast cancer and the environment," International Journal of Occupational and Environmental Health **15**(1), 43–78 (2009).
47. P. Chien, T. Suzuki, M. Tsuji, M. Ye, I. Minami, K. Toda, H. Otsuka, K. Toma, T. Arakawa, and K. Araki, "Biochemical gas sensors (bio sniffers) using forward and reverse reactions of secondary alcohol dehydrogenase for breath isopropanol and acetone as potential volatile biomarkers of diabetes mellitus," Anal. Chem. **89**(22), 12261–12268 (2017).
48. P. Zhao, T. D. Bennett, N. P. Casati, G. I. Lampronti, S. A. Moggach, and S. A. Redfern, "Pressure-induced oversaturation and phase transition in zeolitic imidazolate frameworks with remarkable mechanical stability," Dalton Trans. **44**(10), 4498–4503 (2015).
49. L. Ma, Z. Rui, Q. Wu, H. Yang, Y. Yin, Z. Liu, Q. Cui, and H. Wang, "Performance evaluation of shaped MIL-101(Cr) –ethanol working pair for adsorption refrigeration," Appl. Therm. Eng. **95**, 223–228 (2016).
50. G. Férey, C. Mellot-Draznieks, C. Serre, F. Millange, J. Dutour, S. Surblé, and I. Margiolaki, "A chromium terephthalate-based solid with unusually large pore volumes and surface area," Science **309**(5743), 2040–2042 (2005).
51. J. Cortés-Súarez, V. Celis-Arias, H. I. Beltrán, A. Tejeda-Cruz, I. A. Ibarra, J. E. Romero-Ibarra, E. Sánchez-González, and S. Loera-Serna, "Synthesis and characterization of an SWCNT@ HKUST-1 composite enhancing the CO_2 adsorption properties of HKUST-1," ACS Omega **4**(3), 5275–5282 (2019).
52. J. Cousin Saint Remi, T. Rémy, V. Van Hunskerken, S. van de Perre, T. Duerinck, M. Maes, D. De Vos, E. Gobechiya, C. E. A. Kirschhock, G. V. Baron, and J. F. M. Denayer, "Biobutanol separation with the metal–organic framework ZIF-8," ChemSusChem **4**(8), 1074–1077 (2011).
53. Y. Mao, J. Cheng, H. Guo, Y. Shao, L. Qian, and W. Yang, "Sulfamic acid–modified zeolitic imidazolate framework (ZIF-90) with synergetic Lewis and Brønsted acid sites for microalgal biodiesel production," Fuel **331**, 125795 (2023).
54. P. F. Liguori, B. Russo, A. Melicchio, and G. Golemme, "Synthesis and gas sorption behaviour of ZIF-90 with large pore volume," New J. Chem. **41**(22), 13235–13239 (2017).
55. L. Dong, K. Zhao, J. Wu, G. Deng, C. Tang, C. Zhang, H. Xu, Q. Wang, K. Chen, and K. S. Chiang, "A vapochromic dye/graphene coated long-period fiber grating for benzene vapor sensing," Mater. Chem. Front. **6**(17), 2438–2446 (2022).
56. Z. Li, J. Liu, H. Wu, J. Tang, Z. Li, Y. Xu, F. Zhou, and W. Liu, "Photonic Crystals Constructed by Isostructural Metal-organic Framework Films," Nano Research, (2023).

Optics EXPRESS

57. M. Njegovec and D. Donlagic, "A fiber-optic gas sensor and method for the measurement of refractive index dispersion in NIR," Sensors **20**(13), 3717 (2020).
58. Y. Cheng, H. Luo, F. Chen, and R. Gong, "Triple narrow-band plasmonic perfect absorber for refractive index sensing applications of optical frequency," OSA Continuum **2**(7), 2113–2122 (2019).
59. C. Zhu, Y. Zhuang, and J. Huang, "Sensitivity-Enhanced Fiber-Optic Sensor in a Microwave Photonics Fiber Loop Ringdown System," J. Lightwave Technol. **40**(16), 5768–5774 (2022).
60. H. Fujiwara, "*Spectroscopic ellipsometry: principles and applications*," John Wiley & Sons (2007).
61. D. Johannsmann, "The quartz crystal microbalance in soft matter research," Soft and Biological Matter, 191–204 (2015).
62. I. Langmuir, "The constitution and fundamental properties of solids and liquids. Part I. Solids," J. Am. Chem. Soc. **38**(11), 2221–2295 (1916).
63. K. Y. Foo and B. H. Hameed, "Insights into the modeling of adsorption isotherm systems," Chem. Eng. J. **156**(1), 2–10 (2010).
64. J. Wu, W. Zhang, Y. Wang, B. Li, H. Ting, Y. Zheng, L. Jiang, K. Chen, and K. S. Chiang, "Nanoscale light–matter interactions in metal–organic frameworks cladding optical fibers," Nanoscale **12**(18), 9991–10000 (2020).
65. A. Demessence, P. Horcajada, C. Serre, C. Boissière, D. Grosso, C. Sanchez, and G. Férey, "Elaboration and properties of hierarchically structured optical thin films of MIL-101 (Cr)," Chem. Commun. **46**(46), 7149–7151 (2009).
66. M. D. Allendorf, R. J. Houk, L. Andruszkiewicz, A. A. Talin, J. Pikarsky, A. Choudhury, K. A. Gall, and P. J. Hesketh, "Stress-induced chemical detection using flexible metal− organic frameworks," J. Am. Chem. Soc. **130**(44), 14404–14405 (2008).
67. S. Truax, K. S. Demirci, L. A. Beardslee, Y. Luzinova, A. Hierlemann, B. Mizaikoff, and O. Brand, "Mass-sensitive detection of gas-phase volatile organics using disk micro resonators," Anal. Chem. **83**(9), 3305–3311 (2011).
68. Y. Lü, W. Zhan, Y. He, Y. Wang, X. Kong, Q. Kuang, Z. Xie, and L. Zheng, "MOF-templated synthesis of porous Co_3O_4 concave nanocubes with high specific surface area and their gas sensing properties," ACS Appl. Mater. Interfaces **6**(6), 4186–4195 (2014).